atmosphere

MDPI

Article

A Study of the Characteristics of Vertical Cloud Base Height Distribution over Eastern China

Jiwei Xu [1,2], Dong Liu [1,2,*], Zhenzhu Wang [1,2], Decheng Wu [1], Siqi Yu [1,2] and Yingjian Wang [1,2]

[1] Key Laboratory of Atmospheric Optics, Anhui Institute of Optics and Fine Mechanics, Chinese Academy of Sciences, Hefei 230031, Anhui, China; xujw14@mail.ustc.edu.cn (J.X.); zzwang@aiofm.ac.cn (Z.W.); dchwu@aiofm.ac.cn (D.W.); yusq@mail.ustc.edu.cn (S.Y.); wyj@aiofm.ac.cn (Y.W.)

[2] University of Science and Technology of China, Hefei 230026, Anhui, China

* Correspondence: dliu@aiofm.cas.cn

Received: 9 May 2019; Accepted: 31 May 2019; Published: 4 June 2019

Abstract: Cloud is an important factor that affects weather and climate, and the vertical distribution of cloud determines its role in the atmospheric radiation transfer process. In this paper, the characteristics of different cloud types and their vertical cloud base height distributions over Eastern China are investigated with a four-year 2B-CLDCLASS-LIDAR product. The intercomparison of cloud base height distribution from ground-based lidar, CloudSat and CALIPSO measurements was studied with observations over the Hefei and Jinhua areas. The 2B-CLDCLASS-LIDAR product has the potential to uncover geographical and seasonal changes in cloud base height distribution over the Hefei area and Jinhua area, which may be beneficial for local climate models, although the CPR on CloudSat suffers from surface clutter or blind-zones. The results show that for non-precipitation cloud over the defined region (Eastern China), the occurrence frequencies of altocumulus, stratocumulus, and cirrus clouds are 29.4%, 21.0%, and 18.9%, respectively. The vertical occurrence frequencies of their cloud base heights are 0.5–8.5 km, below 3.5 km, and 5.5–17.0 km. The precipitation clouds are dominated by nimbostratus (48.4%), cumulus (17.9%), and deep convective clouds (24.2%), and their cloud base heights are all below 3.0 km. The cloud base height distributions have large differences below 3 km between the satellite measurement and ground-based measurement over Hefei site. Between the Hefei site and Jinhua site, the difference in cloud base height distribution measured by ground-based lidar is in good agreement with that measured by satellite over their matched grid boxes. Over the Hefei site, the vertical occurrence frequencies of cloud base height measured by ground-based lidar are higher than the satellite measurement within 0–0.5 km during all the seasons. It is suggested that more cloudy days may result from the sufficient water vapor environment in Hefei. In summer, the occurrence frequency of the cloud base height distribution at a height of 0–2.0 km is lower than other seasons over Jinhua city, which may be associated with the local weather system. Over the Jinhua site, the difference in seasonal cloud base height distribution based on satellite is in good agreement with that based on ground-based lidar. However, it does not appear over Hefei site. Thus, a multi-platform observation of cloud base height seems to be one of the essential ways for improvement in the observation of cloud macroscopic properties.

Keywords: cloud base height; cloud type; Eastern China; 2B-CLDCLASS-LIDAR; lidar

1. Introduction

The extensive distribution of cloud macro-physical properties has an important effect on the cloud radiative effect associated with the atmospheric radiation transfer process, and on the cloud

precipitation associated with the water cycle process. The cloud amount, cloud height (base and top), and the occurrence time determine the cloud radiative effect [1–3]. During daytime, the cloud type and cloud height determine the cool or warm effect of a cloud to the surface [4]. At night, almost all types of clouds have a warming effect. However, our knowledge of cloud processes, which is one of the largest uncertainties in cloud parameterization for simulating models in atmospheric circulation and climate change [5,6], is inadequate. A long-term observation of the cloud is essential. Satellite observations provide an opportunity to assess cloud processes from a global perspective [7–9]. Cloud profiling radar on-board the CloudSat satellite combined with cloud-aerosol lidar on-board the CALIPSO satellite can scan the cloud from space and produce cloud products with complementary advantages of laser and microwave measurement for the cloud vertical structure [10–12]. Cloud vertical structure is relevant to the cloud micro-physical properties as well [13]. Cloud base height is one of the fundamental cloud variables of cloud vertical structure [14].

Except for detection in space, ground-based detections by using lidar have made a sizeable effort and contribution to monitoring the macro-physical properties of clouds, based on lidar networks [14,15]. Several researchers have studied the remote sensing of cloud vertical structure using CloudSat, CALIPSO, and ground-based observation together. Kim et al. reported that the cloud base height derived from the Cloud Profiling Radar (CPR) and ground-based lidar are generally in good agreement with each other (coefficient of determination in linear relationship, ~0.996) [16]. A good agreement in cloud top height and cloud base height with cirrus cloud optical depth between ground-based lidar and space-borne Cloud-Aerosol Lidar with Orthogonal Polarization (CALIOP) was found in Seoul, Korea [17]. Blanchard et al. [18] reported that cloud fraction occurrences from ground-based instruments correlated well with both CALIPSO operational products and combined CALIPSO-CloudSat retrievals, with a hit rate of 85%, and misdetections were mainly attributed to sensitivity loss and distance between the satellite track and the station. Comparisons of cloud base height detected by ceilometers and CALIPSO were also carried out in the southern Appalachian mountains [19].

With regard to the accurate estimation of variations in local cloud and the parameterization of local cloud models, observation samples of satellites are comparatively sparse. It is necessary to compare the cloud base height measured by the satellite with the ground-based detection. Thus, we collect the 2B-CLDCLASS-LIDAR product data and ground-based lidar data measured over Jinhua site or Hefei site to investigate the distribution of cloud base height over Eastern China. Section 2 describes the 2B-CLDCLASS-LIDAR product and the method used to determine the cloud base height from lidar data. In Section 3, the relationship between cloud base height and cloud type is investigated. The comparisons of vertical cloud base height distribution measured by 2B-CLDCLASS-LIDAR with ground-based lidar observations are given in Section 3. Finally, a summary and conclusions are presented in Section 4.

2. Experiments and Methods

The cloud measurement products CloudSat and CALIPSO were collected for study. The level 2 cloud scenario classification product 2B-CLDCLASS-LIDAR [8], which combines CPR and CALIOP from CloudSat and CALIPSO, provided the information on cloud type, cloud base height, and cloud precipitation (the product is available from the website http://www.cloudsat.cira.colostate.edu/data-products/level-2b/2b-cldclass-lidar). Four-year 2B-CLDCLASS-LIDARdata from 2007 to 2010 was used in this paper. The parameter "PrecipitationFlag" of 2B-CLDCLASS-LIDAR can be used to classify the precipitation situations of cloud layers. The number "0" for "PrecipitationFlag" represents a cloud with no precipitation. Numbers "1, 2, 3" for "PrecipitationFlag" mark the cloud layers with liquid precipitation, solid precipitation, and possible drizzle, respectively, which are regarded as precipitation cloud layers. The cloud types in 2B-CLDCLASS-LIDAR are identified as stratus (St), stratocumulus (Sc), cumulus (Cu, including cumulus congestus), nimbostratus (Ns), altocumulus (Ac), altostratus (As), deep convective (cumulonimbus), or high (cirrus and cirrostratus) cloud based on the "CloudLayerType" parameter. The "CloudLayerBase" stores the cloud base height information of a

detected cloud layer. The research region, Eastern China, is limited from 25.0° N to 35.0° N and 110.0° E to 122.5° E, which mostly consists of land regions (see Figure 1). We divided this area into grid boxes of 1.0° × 1.0° in latitude and longitude.

In the defined region, two lidar observation sites (see Figure 1) had been set up to measure the vertical structure of macro- and micro-physical properties of aerosols and clouds. The National Institute for Environmental Studies (NIES) lidar in the Hefei site had thirty months of observation data from January 2012 to October 2014 [20,21]. This lidar had three channels at wavelengths of 532 nm and 1064 nm and depolarization at 532 nm. The vertical resolution was 7.5 m and time resolution was 15 min, with a signal accumulation of 3000 shots in 5 minutes. The operated lidar in Jinhua site was the Dual-wavelength Mie Polarization Raman Lidar (DMPRL) system [22], emitting laser pulses at 532 nm and 1064 nm, with a repetition rate of 20 Hz. The elastic scattered signals, including depolarization at 532 nm and Raman scattered signal at 607 nm, can be received simultaneously. The vertical resolution was 7.5 m and time resolution was 30 s. The DMPRL was used for detection during June 2013 to July 2014 in Jinhua area.

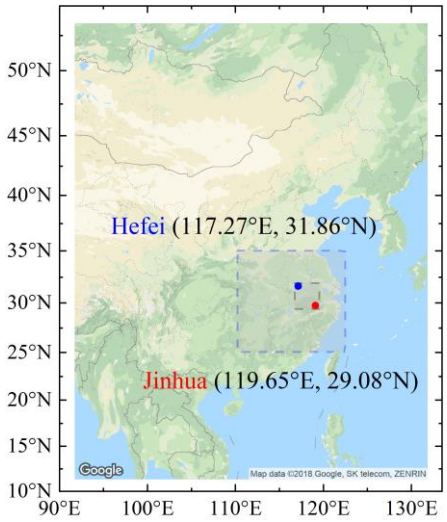

Figure 1. The region defined in this study is shaded by a rectangle with dashed lines. The two lidar observation sites are marked with the blue dot (Hefei) and red dot (Jinhua), respectively. The smaller rectangle is used in Figure 7c.

There are many methods to determine the cloud base height from lidar signals such as the differential zero-crossing method [23], threshold method [23–25], multiscale detection algorithm [26], semidiscretization processing technique [27], and so on [12,28]. One of the tough problems of cloud layer determination from lidar signal profiles is the treatment of noise. All the above methods more or less eliminate noise in different ways. In this study, every tiny feature is distinguished using a differential zero-crossing method, as before [29]. Then, the feature layers can be identified as cloud layers or aerosol layers. Furthermore, the volume depolarization ratio (VDR) profiles at 532 nm are used in some scenes to improve the accuracy of identified cloud results. The detailed algorithm flow is shown in Figure 2. What needs to be mentioned is that we set three thresholds for clouds in different situations. In terms of general cloud (middle-level cloud), it has the apparent differentia of the value of feature peak return signal (RS) minus feature base RS, compared to the aerosol layer. For lower clouds, they always have an obvious attenuation to lidar signal, and their effective cloud top height, which is lower than the real cloud top height, can be measured due to the fact that the laser goes through the cloud and decreases to the background signal level. For thin cloud appearing at high altitude, it is hard to be discriminated from the aerosol layer due to the weak return signal, however, the VDR has a great advantage in this task [30]. Figure 3 illustrates the process of cloud layer detection. The initial

search height is 150 m, which is the top height of the blind area. The threshold value of an averaged cloud layer VDR is 0.1 for high cloud or cirrus cloud.

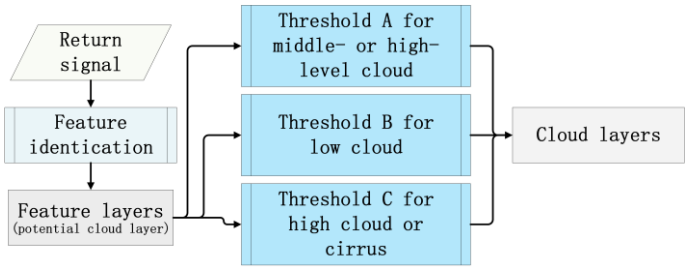

Figure 2. Flow chart of the cloud layer detection algorithm.

The cloud occurrence frequency (F_{cloud}) is derived from the ratio of the number of cloud occurrences N_{cloud} per grid box over the number of observations N_{profiles} in that grid box: $F_{\text{cloud}} = N_{\text{cloud}} / N_{\text{profiles}}$. It can be used to derive the occurrence frequency F_X of a given cloud type X. The occurrence frequency of cloud base height is derived by the same method for each grid box: $F_{\text{CBH}} = N_{\text{bin}} / N_{\text{total}}$. The N_{bin} and N_{total} represent the number of cloud base of eight types in each bin, divided from vertical space (0–20 km) at a step of 0.5 km, and the total number in all bins, respectively. This method is applied for every season to derive a seasonally averaged frequency in every grid box.

In our study, if multi-layer cloud appeared, we only considered the first cloud layer. This is because, on the one hand, the lidar signal suffers from extinction, preventing it from detecting any other upper cloud layers. On the other hand, the combined CALIPSO and CloudSat cloud product (2B-CLDCLASS-LIDAR) can describe multi-layer cloud depending on CPR, due to its advantage of cloud penetration capability. The satellite observation time over the defined region was limited (always midnight and noon at local standard time), hence, the cloud fraction measured by the satellite or ground-based observation was unmatched. Therefore, to reduce this influence, the ground-based observation time was limited during 13:00–15:00 and 1:00–3:00 at local standard time (LST). The year timeframe difference and its influence among the three observation databases is illustrated in Section 3.

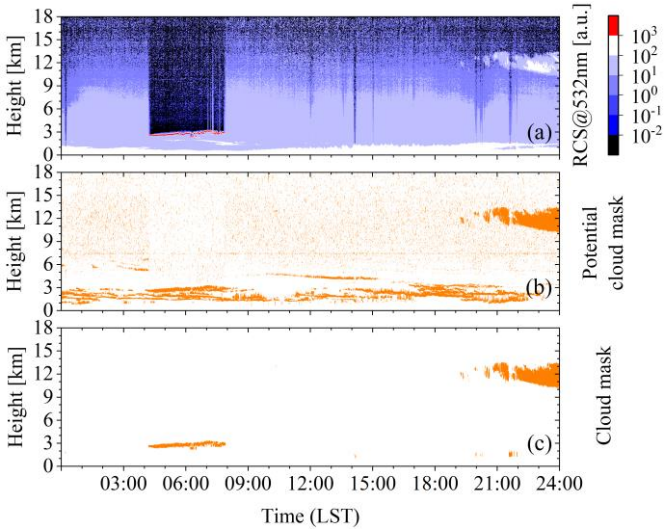

Figure 3. A case of cloud layer detection: (**a**) The range-corrected signal at 532 nm; (**b**) the potential cloud mask after feature identification; (**c**) the cloud mask represents the cloud layers. This case was measured in Jinhua on June 5, 2013.

3. Results

The geographical distributions of normal profile number and cloud fraction derived over 2007–2010 are shown in Figure 4. The normal profile number is defined as the ratio of the amount of profiles in a single 1.0° × 1.0° grid box to the maximal amount of all grid boxes in the defined region. The maximal amount of profiles is 15237. In Figure 4a, it clearly shows that the seasonal variation can be derived based on about 2000–3000 profiles in each grid box. Figure 4b shows the heterogeneity in geographical distribution. The grid containing Jinhua site has a larger cloud fraction than that of the grid containing Hefei site.

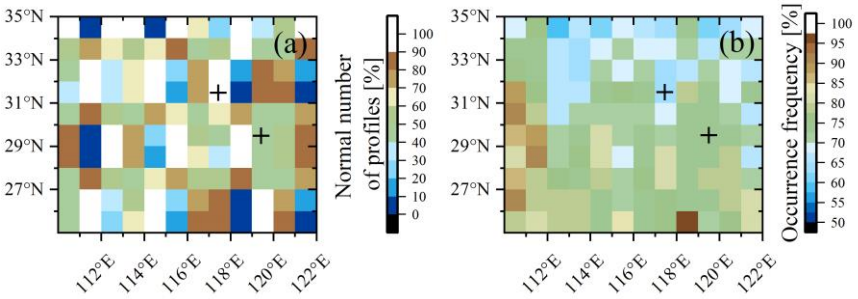

Figure 4. (**a**) Normal number of profiles per grid box. The maximal amount of profiles is 15237; (**b**) The geographical distribution of cloud occurrence frequency; the cross symbols correspond to the lidar sites.

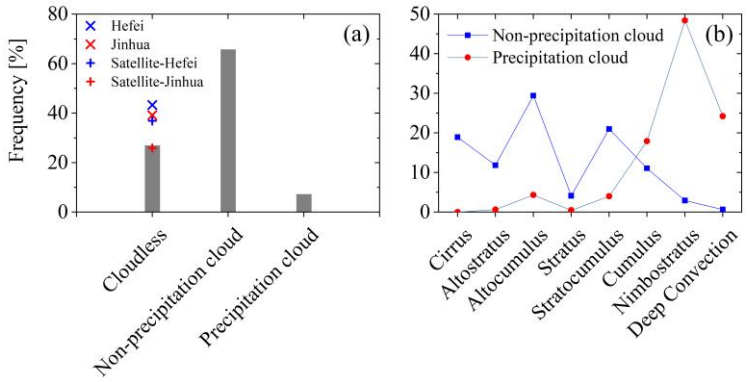

Figure 5. (**a**) Occurrence frequencies of cloudless, non-precipitation cloud, and precipitation cloud. The blue cross sign corresponds to the cloudless occurrence frequency for Hefei lidar site, and the red one for Jinhua lidar site. The cross symbol indicates the matched grid box. (**b**) Occurrence frequencies of eight cloud types for non-precipitation cloud or precipitation cloud.

It is well known that the cloud base height of non-precipitation cloud has an extensive distribution in the vertical direction. In contrast, precipitation cloud has a lower height especially for convective precipitation cloud. Figure 5 shows the occurrence frequency of cloudless, non-precipitation cloud or precipitation cloud (Figure 5a) and the occurrence frequency of eight cloud types of non-precipitation cloud or precipitation cloud (Figure 5b) over the defined region. In Figure 5a, it is obvious that non-precipitation cloud dominates the cloud fraction. The cloudless occurrence frequencies of ground-based lidars over Hefei site (which is very close to the result in a previous study [21]) and Jinhua site are higher than that of 2B-CLDCLASS-LIDAR over the defined region. However, the grid box containing Hefei site has a better agreement with the ground-based lidar measurement than the equivalent comparison for Jinhua. The difference in Jinhua site is because the grid box area is larger than a single-point and because of the variability in year-average cloud fraction among the different year timeframes. In Figure 5b, for precipitation cloud, the occurrence frequency of cumulus, nimbostratus, and deep convection cloud, collectively, is higher than 17%. As for non-precipitation cloud, the occurrence frequency of cirrus, altocumulus, and stratocumulus cloud, collectively, is

higher than 18%. That is to say, the contributions to cloud base height of cirrus, altocumulus, and stratocumulus clouds of non-precipitation cloud cannot be ignored in the cloud base distribution.

3.1. Cloud Base Height and Cloud Type

Over the defined region, the cloud base height parameter of the 2B-CLDCLASS-LIDAR product can be used to investigate the relationships between cloud base height and cloud type. Figure 6 shows the occurrence frequencies of cloud base height for eight cloud types. For non-precipitation cloud in Figure 6a, the occurrence frequency of cloud base height can be divided into three types, including high type, middle type, and low type. The cirrus cloud can be regarded as the high type, with the range of cloud base height from 5.5 to 17 km. The middle type consists of altostratus cloud and altocumulus cloud, with the cloud base height ranging from 0.5 to 8.5 km. The other cloud types with cloud base heights below 3.5 km are regarded as low cloud. As for the precipitation cloud in Figure 6b, with the peak in occurrence frequency at 1 to 1.5 km, the cloud base heights for all of the eight cloud types are below 3 km.

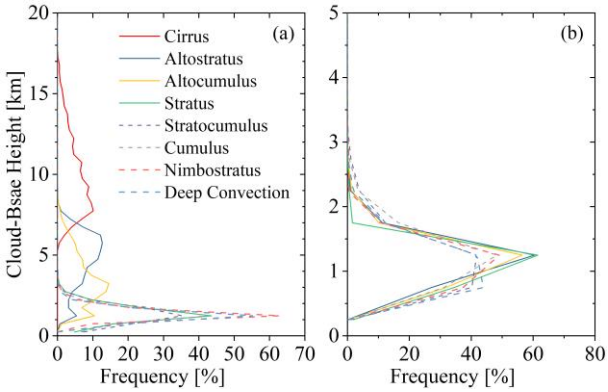

Figure 6. Occurrence frequencies of cloud base heights for eight cloud types: (**a**) Non-precipitation cloud; (**b**) precipitation cloud.

3.2. Comparison of Cloud Base Height Distribution between Two Ground-Based Observation Sites

The retrieval method of cloud base heights from lidar data is described in Section 2. Unfortunately, the observation time of the lidar data is later than the 2B-CLDCLASS-LIDAR product data. Therefore, we attempt to counterbalance the influence of the timeframe problem in this study. Figure 7 shows the occurrence frequency of cloud base height derived from ground-based lidars in Hefei and Jinhua sites and from 2B-CLDCLASS-LIDAR in matched grid boxes. The cloud base height occurrence frequency of 2B-CLDCLASS-LIDAR or ground-based lidar over Jinhua city has good consistency in the vertical cloud base height distribution. For the ground-based lidar in Hefei city, the occurrence frequency of cloud base height is different at 11 km and below 3 km. There may be three reasons here for this. The first is year variation (timeframe problem). Because of the different year timeframes of the three databases, the difference between the lidar measurement and the matched grid box will be enlarged. Figure 7c illustrates the standard deviations of cloud base height distributions during the four years. The cloud base height distribution near 1 km has a larger fluctuation in each season. However, below 1.5 km, the differences between ground-based lidars and satellites are larger than the year variations, which may be caused by the two reasons below. The second reason is from lidar measurement. The single-point observation has a representativeness problem. The third reason is from satellite measurement. The Surface clutter or blind-zone of the radar on CPR brings about the misdetection of the lower cloud layers. The first and third reasons need to be highly considered.

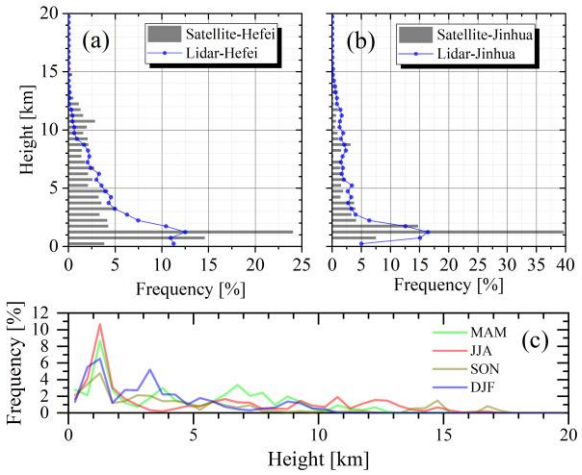

Figure 7. Occurrence frequency of cloud base height measured by CALIPSO and CloudSat or by ground-based lidar: (**a**) Hefei site; (**b**) Jinhua site; (**c**) the standard deviations of cloud base height distribution during the four years and the grid boxes area (smaller rectangle) are shown in Figure 1.

The detailed differences in cloud base height distribution between the two ground-based observation sites are shown in Figure 8. In Figure 8b, Hefei site has a decreasing frequency of the cumulus and stratocumulus cloud fractions, which leads to the decreasing frequency of cloud base height at 1–2 km (see Figure 8a) in both ground-based lidar and satellite measurement, because the cloud base heights of cumulus and stratocumulus contribute to the cloud base height distribution at about 0–3 km (see Figure 6). Hefei site has an increasing frequency of cirrus cloud fraction, however the ground-based lidar measurement has an inverse change at about 11 km. This is because the laser energy of lidar in Hefei city is weaker than that in Jinhua city, which results in the missing measurement of the cirrus cloud over Hefei area. It is obvious that satellite and ground-based lidar measurements have a good agreement for the change in cloud base height distribution between the two sites, which indicates that the 2B-CLDCLASS-LIDAR can appropriately distinguish the cloud type fraction change between the two sites. The large divergence between the two measurements at about 1–2 km may result from yearly variation.

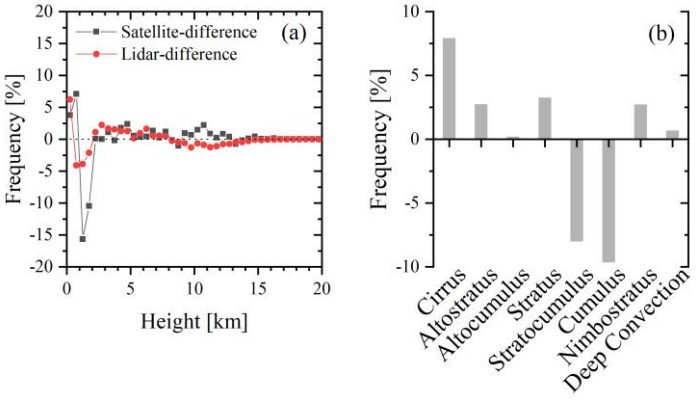

Figure 8. (**a**) Occurrence frequencies of cloud base height between the two observation sites; (**b**) Occurrence frequencies of cloud types between the two observation sites. The columns above the horizontal axis indicate an increase in the Hefei site.

3.3. Seasonal Variation in Cloud Base Height Based on Satellite and Ground-Base Observations

To respectively investigate the seasonal variation in cloud base height distribution for the satellite and ground-based observations in the two sites, Figure 9 shows the seasonal occurrence frequencies of cloud base height in four seasons. Over Hefei site, the cloud with cloud base height at 0–0.5 km

(cumulus [7]) has a higher frequency in 2B-CLDCLASS-LIDAR, whose difference is higher than the yearly variation at the corresponding height (see Figure 7c). This is probably because the persistent high humidity environment [31] brings more rainy days. This phenomenon is more obvious in the monsoon period [32] (see Figure 9b,d). However, this phenomenon does not appear in the satellite measurement. In summer over Jinhua area, the East Asian monsoon does not bring more low clouds to the contrary, it brings less low clouds (see Figure 9f) due to the control of the western North Pacific subtropical high after the plum rain season. The difference correlations for seasonal variation in cloud base height distribution between the satellite and ground-based observations in the two sites are shown in Figure 10. The difference for seasonal variation in cloud base height distribution is derived from the frequencies of the cloud base height minus the averaged seasonal fraction during the four seasons. Over Hefei site, the slope of linear fitting is 0.55, which is less than that in Jinhua site. The grid box containing Jinhua site has a clearer description of the seasonal change in cloud base height distribution in Jinhua site, although the year variation effect exists here. More comparisons between them should be presented.

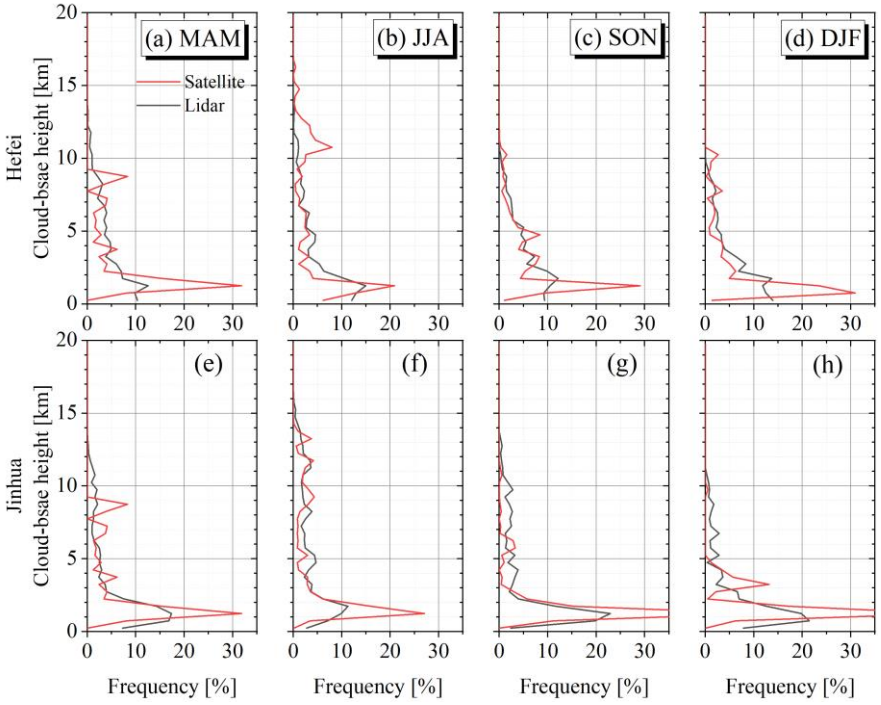

Figure 9. Seasonal occurrence frequency of cloud base height measured by CALIPSO and CloudSat or ground-based lidar. (**a**–**d**) represent four-season results over Hefei site. (**e**–**h**) represent four-season results over Jinhua site.

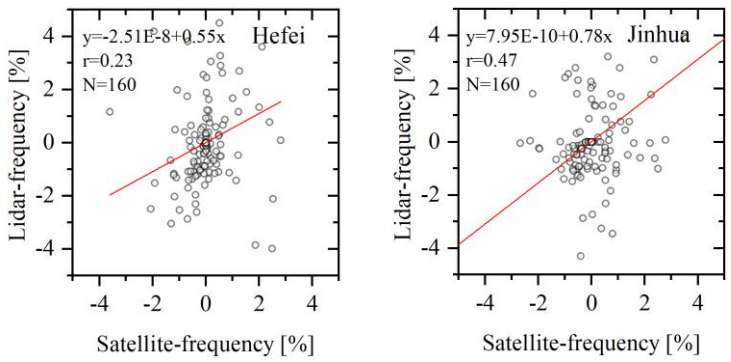

Figure 10. Seasonal occurrence frequency of cloud base height measured by CALIPSO and CloudSat or ground-based lidar.

4. Conclusions

The vertical distribution of cloud base height is an essential element for the radiation process and the climate model. We used the 2B-CLDCLASS-LIDAR product, which combines CloudSat and CALIPSO, and observational data from ground-based lidars to investigate the vertical distribution of cloud base height over the defined region (Eastern China). The method described in Section 2 is used to retrieve the cloud base height from lidar measurements. The clouds are classified into precipitation and non-precipitation clouds to investigate the occurrence frequencies of eight cloud types and their cloud base heights. The occurrence frequency of non-precipitation cloud is dominated by altocumulus, stratocumulus, and cirrus clouds. The precipitation clouds have higher occurrence frequencies in nimbostratus, cumulus, and deep convective clouds. The occurrence frequencies of vertical cloud base height distribution measured by the two lidar sites are compared with the 2B-CLDCLASS-LIDAR product, as well as the seasonal results. The difference in occurrence frequencies of cloud types between the two sites is in good agreement with the difference in cloud base height distribution between the two sites, based on either satellite or ground-based measurements. The seasonal results for vertical cloud base height distribution over Jinhua area and Hefei area indicate the influences of local climate on cloud base height distribution. The difference in seasonal occurrence frequencies of cloud base height distributions between lidar and satellite measurements in Jinhua site indicates the seasonal resolution of cloud base height distribution by the 2B-CLDCLASS-LIDAR product. Therefore, the 2B-CLDCLASS-LIDAR product has the ability to differentiate the variations in cloud type fraction associated with the cloud base height distribution between the two sites, however the ability to differentiate the seasonal changes in cloud base height distribution is only potential in Jinhua site and is insufficient in Hefei site. Of course, the different timeframes is a negligible factor, which needs to be improved in future studies. The main reasons for the insufficiency aspect may be the limitations of CPR in the lower cloud layer.

Cloud is the product of a dynamic and thermodynamic coupling process under local and large-scale climate influences. Lidar is a powerful tool to continuously monitor the cloud process. The gradually improving lidar network brings the possibility of complementation between satellite and ground-based observations of cloud macro-physical properties. The comparison of vertical cloud base height distribution is beneficial to this complementation. In addition, the understanding of the cloud base height distribution is important for the study of local weather models. The combined satellite and ground-based observations can better uncover the geographical and seasonal distribution of cloud base height. Therefore, in future studies we will compare more areas and look for the differences between these regions.

Author Contributions: The first author conducted the data analysis and manuscript writing. The second author provided direction to this paper. All the authors analyzed the results and revised the manuscript.

Acknowledgments: This research was supported by the International Partnership Program of Chinese Academy of Sciences (Grant No. 116134KYSB20180114), and by the National Key R&D Program of China (Grant No. 2018YFB0504500) and funded by the Science and Technology Service Network Initiative (STS) under No. KFJ-STS-QYZD-022, and by the Youth Innovation Promotion Association CAS (2017482). The authors thank Prof. Zhien Wang of University of Colorado Boulder for the improvement advice to this paper. The authors would like to thank the Cooperative Institute for Research in the Atmosphere (CIRA) CloudSat Processing Data Center (DPC) for the CloudSat data (http://www.cloudsat.cira.colostate.edu), and the Atmospheric Science Data Center (ASDC) for CALIPSO data (https://www-calipso.larc.nasa.gov/).

Conflicts of Interest: The authors declare no conflict of interest.

References

1. Ramanathan, V.; Cess, R.D.; Harrison, E.F.; Minnis, P.; Barkstrom, B.R.; Ahmad, E.; Hartmann, D. Cloud-radiative forcing and climate: Results from the Earth radiation budget experiment. *Science* **1989**, *243*, 57–63. [CrossRef] [PubMed]
2. Zhang, J.; Li, Z.; Chen, H.; Yoo, H.; Cribb, M. Cloud vertical distribution from radiosonde, remote sensing, and model simulations. *Clim. Dyn.* **2014**, *43*, 1129–1140. [CrossRef]

3. Yan, Y.; Liu, Y.; Lu, J. Cloud Vertical Structure, Precipitation, and Cloud Radiative Effects over Tibetan Plateau and its Neighboring Regions: Cloud and CRE over Tibetan Plateau. *J. Geophys. Res. Atmos.* **2016**, *121*, 5864–5877. [CrossRef]
4. Lee, W.-H.; Iacobellis, S.F.; Somerville, R.C.J. Cloud Radiation Forcings and Feedbacks: General Circulation Model Tests and Observational Validation. *J. Clim.* **1997**, *10*, 2479–2496. [CrossRef]
5. Zhang, M.H.; Lin, W.Y.; Klein, S.; Bacmeister, J.T.; Bony, S.; Cederwall, R.T.; Del Genio, A.D.; Hack, J.J.; Loeb, N.G.; Lohmann, U.; et al. Comparing clouds and their seasonal variations in 10 atmospheric general circulation models with satellite measurements. *J. Geophys. Res. Space Phys.* **2005**, *110*, 1637–1639. [CrossRef]
6. Bony, S.; Colman, R.; Kattsov, V.M.; Allan, R.P.; Bretherton, C.S.; Dufresne, J.-L.; Hall, A.; Hallegatte, S.; Holland, M.M.; Ingram, W.; et al. How Well Do We Understand and Evaluate Climate Change Feedback Processes? *J. Clim.* **2006**, *19*, 3445–3482. [CrossRef]
7. Sassen, K.; Wang, Z. Classifying clouds around the globe with the CloudSat radar: 1-year of results. *Geophys. Res. Lett.* **2008**, *35*, 35. [CrossRef]
8. Sassen, K.; Wang, Z.; Liu, D. Global distribution of cirrus clouds from CloudSat/Cloud-Aerosol Lidar and Infrared Pathfinder Satellite Observations (CALIPSO) measurements. *J. Geophys. Res. Space Phys.* **2008**, *113*, 113. [CrossRef]
9. Zhang, D.; Wang, Z.; Liu, D. A global view of midlevel liquid-layer topped stratiform cloud distribution and phase partition from CALIPSO and CloudSat measurements. *J. Geophys. Res. Space Phys.* **2010**, *115*, 115. [CrossRef]
10. Venema, V.; Russchenberg, H.; Apituley, A.; Van Lammeren, A.; Ligthart, L. Cloud boundary height measurements using lidar and radar. *Phys. Chem. Earth Part B Hydrol. Oceans Atmos.* **2000**, *25*, 129–134. [CrossRef]
11. Liu, Y.; Shupe, M.D.; Wang, Z.; Mace, G. Cloud vertical distribution from combined surface and space radar/lidar observations at two Arctic atmospheric observations. *Atmospheric Chem. Phys. Discuss.* **2017**, *17*, 1–28. [CrossRef]
12. Wang, Z.; Sassen, K. Cloud Type and Macrophysical Property Retrieval Using Multiple Remote Sensors. *J. Appl. Meteorol.* **2001**, *40*, 1665–1682. [CrossRef]
13. Donovan, D.P.; Van Lammeren, A.C.A.P. Cloud effective particle size and water content profile retrievals using combined lidar and radar observations: 1. Theory and examples. *J. Geophys. Res. Space Phys.* **2001**, *106*, 27425–27448. [CrossRef]
14. Hirsch, E.; Agassi, E.; Koren, I. A novel technique for extracting clouds base height using ground based imaging. *Atmos. Meas. Tech.* **2011**, *4*, 117–130. [CrossRef]
15. Dupont, J.-C.; Haeffelin, M.; Morille, Y.; Comstock, J.M.; Flynn, C.; Long, C.N.; Sivaraman, C.; Newson, R.K. Cloud properties derived from two lidars over the ARM SGP site. *Geophys. Res. Lett.* **2011**, *38*. [CrossRef]
16. Kim, S.-W.; Chung, E.-S.; Yoon, S.-C.; Sohn, B.-J.; Sugimoto, N. Intercomparisons of cloud-top and cloud-base heights from ground-based Lidar, CloudSat and CALIPSO measurements. *Int. J. Remote. Sens.* **2011**, *32*, 1179–1197. [CrossRef]
17. Kim, Y.; Kim, S.-W.; Kim, M.-H.; Yoon, S.-C. Geometric and optical properties of cirrus clouds inferred from three-year ground-based lidar and CALIOP measurements over Seoul, Korea. *Atmos. Res.* **2014**, *139*, 27–35. [CrossRef]
18. Blanchard, Y.; Pelon, J.; Eloranta, E.W.; Moran, K.P.; Delanoë, J.; Sèze, G. A Synergistic Analysis of Cloud Cover and Vertical Distribution from A-Train and Ground-Based Sensors over the High Arctic Station Eureka from 2006 to 2010. *J. Appl. Meteorol. Clim.* **2014**, *53*, 2553–2570. [CrossRef]
19. Duan, Y.; Barros, A.P. Understanding How Low-Level Clouds and Fog Modify the Diurnal Cycle of Orographic Precipitation Using In Situ and Satellite Observations. *Remote. Sens.* **2017**, *9*, 920. [CrossRef]
20. Wang, Y.; Sun, L.; Liu, D.; Xie, C. Cloud and Aerosol Interaction Observed in SKYNET Hefei Site in China. *EPJ Web Conf.* **2016**, *119*, 16013. [CrossRef]
21. Sun, L.; Liu, D.; Wang, Z.; Wang, Z.; Wu, D.; Bo, G.; Wang, Y. Cloud vertical structures detected by lidar and its statistical results at HeRO site in Hefei, China. In Proceedings of the SPIE—The International Society for Optical Engineering 2014, Beijing, China, 13–16 October 2014.
22. Yu, S.; Liu, D.; Wang, Z.; Xu, J.; Tian, X.; Wu, D.; Xie, C.; Wang, Y. Measurements of aerosol layer height and vertical profiles by lidar over Jinhua City. *Int. Soc. Opt. Photonics* **2017**. [CrossRef]

23. Platt, C.M.; Young, S.A.; Carswell, A.I.; Pal, S.R.; McCormick, M.P.; Winker, D.M.; DelGuasta, M.; Stefanutti, L.; Eberhard, W.L.; Hardesty, M.; et al. The Experimental Cloud Lidar Pilot Study (ECLIPS) for Cloud—Radiation Research. *Bull. Am. Meteorol. Soc.* **1994**, *75*, 1635–1654. [CrossRef]
24. Clothiaux, E.E.; Mace, G.G.; Ackerman, T.P.; Kane, T.J.; Spinhirne, J.D.; Scott, V.S. An Automated Algorithm for Detection of Hydrometeor Returns in Micropulse Lidar Data. *J. Atmos. Ocean. Technol.* **1998**, *15*, 1035–1042. [CrossRef]
25. Thorsen, T.J.; Fu, Q.; Newsom, R.K.; Turner, D.D.; Comstock, J.M. Automated Retrieval of Cloud and Aerosol Properties from the ARM Raman Lidar. Part I: Feature Detection. *J. Atmos. Ocean. Technol.* **2015**, *32*, 1977–1998. [CrossRef]
26. Mao, F.; Gong, W.; Zhu, Z. Simple multiscale algorithm for layer detection with lidar. *Appl. Opt.* **2011**, *50*, 6591. [CrossRef] [PubMed]
27. Zhao, C.; Wang, Y.; Wang, Q.; Li, Z.; Wang, Z.; Liu, D. A new cloud and aerosol layer detection method based on micropulse lidar measurements. *J. Geophys. Res. Atmos.* **2014**, *119*, 6788–6802. [CrossRef]
28. Wang, Z.; Wu, D.; Liu, D.; Zhou, J. An Algorithm to Determine Aerosol Extinction Below Cirrus Cloud from Mie-LIDAR Signals. *J. Opt. Soc. Korea* **2010**, *14*, 444–450. [CrossRef]
29. Pal, S.R.; Steinbrecht, W.; Carswell, A.I. Automated method for lidar determination of cloud-base height and vertical extent. *Appl. Opt.* **1992**, *31*, 1488. [CrossRef] [PubMed]
30. Chen, W.-N.; Chiang, C.-W.; Nee, J.-B. Lidar ratio and depolarization ratio for cirrus clouds. *Appl. Opt.* **2002**, *41*, 6470. [CrossRef] [PubMed]
31. Zhang, Q.; Singh, V.P.; Li, J.; Chen, X. Analysis of the periods of maximum consecutive wet days in China. *J. Geophys. Res. Space Phys.* **2011**, *116*, D23106. [CrossRef]
32. Zhang, Q.; Zheng, Y.; Singh, V.P.; Luo, M.; Xie, Z. Summer extreme precipitation in eastern China: Mechanisms and impacts. *J. Geophys. Res. Atmos.* **2017**, *122*, 2766–2778. [CrossRef]